Ultra-Massive MIMO Channel Modeling for Graphene-Enabled Terahertz-Band Communications

Chong Han[1], **Josep Miquel Jornet**[2], and **Ian F. Akyildiz**[3]

[1] Shanghai Jiao Tong University, Shanghai, China, Email: chong.han@sjtu.edu.cn
[2] University at Buffalo, The State University of New York, NY, USA, Email: jmjornet@buffalo.edu
[3] Georgia Institute of Technology, Atlanta, GA, USA, Email: ian@ece.gatech.edu

***Abstract*—Terahertz (THz)-band communication (0.1-10 THz) is envisioned as a key wireless technology to satisfy the increasing demand for faster data-rates in beyond 5G systems, thanks to its ultra-broad bandwidth. The very high path loss at THz frequencies and the limited transmission power of THz transceivers impose a major distance limitation for THz wireless communications. To increase the communication distance and the achievable data rates at THz-band frequencies, the concept of Ultra-Massive MIMO (UM-MIMO) has been introduced, which integrates a very large number of nano-antennas (e.g., 1024) in very small footprints (e.g., 1 mm^2). In this paper, an end-to-end model for UM-MIMO communication in the THz band is developed, by accounting for the properties of graphene-based plasmonic nano-antenna arrays and the peculiarities of three-dimensional THz propagation. The developed model is utilized to investigate the performance of the UM-MIMO channel. In particular, the path gain, the array factor and the the wideband capacity for both spatial multiplexing and beamforming regimes are analyzed. The results show that multi-Terabit-per-second links are feasible at distances of up to 20 m when utilizing 1024×1024 UM-MIMO systems at 0.3 THz and 1 THz.**

I. Introduction

Over the last few years, wireless data traffic has drastically increased due to a change in the way today's society creates, shares and consumes information. Wireless data rates have doubled every eighteen months for the last three decades. Following this trend, *Terabit-per-second (Tbps) links* are expected to become a reality within the next five years [1]. *Terahertz-band (*0.1–10 THz*) communication* is envisioned as a key wireless technology to satisfy the need for much higher wireless data rates [2]. The THz band supports huge transmission bandwidths, which range from almost 10 THz for distances below one meter, to multiple transmission windows, each tens to hundreds of GHz wide, for distances in the order of a few tens of meters. Nevertheless, this very large bandwidth comes at the cost of a very high propagation loss [3]. As a result, high-gain directional antennas are needed to communicate over distances beyond a few meters. Recently, the concept of Massive MIMO has been introduced [4]. When moving to the THz band, antennas become even smaller and many more elements can be embedded in the same footprint.

In this direction, we have recently introduced the concept of Ultra-Massive MIMO (UM-MIMO) communications [5], which could integrate a very large number of nano-antennas in very small footprints to increase the communication distance and the achievable data rates at THz-band frequencies. In particular, nanomaterials such as graphene can be utilized to build miniature plasmonic antennas and transceivers [6] for THz communications. The performance of UM-MIMO communications ultimately depends both the capabilities of novel plasmonic nano-antenna arrays as well as the peculiarities of the THz channel. On the one hand, the performance of individual nano-antennas, mutual coupling effects between them and their dynamic control needs to be captured. On the other hand, the impact of spreading, molecular absorption, reflection and scattering at THz frequencies needs to be taken into account [7]. To the best of our knowledge, there is no complete channel model for UM-MIMO communications that captures all the aforementioned properties.

In this paper, we develop a channel model for UM-MIMO communications in the THz band and analyze the capacity of the system in different specific scenarios. Specifically, first, we analyze the properties of graphene-based plasmonic nano-antenna array and introduce the array-of-subarray (AoSA) architecture for THz wireless communications. Furthermore, we develop a model for the three-dimensional (3D) UM-MIMO channel, which includes the THz path gain and array steering vector. Based on the developed models, we proceed to investigate the performance of the UM-MIMO channel. In particular, the path gain, the array factor and the wideband channel capacity with spatial multiplexing as well as beamforming are studied thoroughly.

The remainder of this paper is organized as follows. In Sec. II, the UM-MIMO system model that includes the graphene antennas and the array-of-subarray architecture in the THz band is presented. Then, the UM-MIMO channel model is developed in Sec. III.Using the developed model, we present an in-depth analysis on the UM-MIMO channel characteristics in Sec. IV. Finally, the paper is concluded in Sec. V.

II. Graphene-based Nano-antenna Arrays

In this section, plasmonic nano-antenna arrays are described as the enabling antenna technology for the realization of UM-MIMO communication in the THz band. After describing the main peculiarities of plasmonic nano-antennas based on graphene, an AoSA architecture is proposed to control and operate the antenna array. The characterization of the graphene-based plasmonic nano-antenna arrays as well as the AoSA

978-1-5386-6355-4/18/$31.00 ©2018 IEEE

architecture will be incorporated in the development of the UM-MIMO channel model in Sec. III.

A. Design of Plasmonic Nano-antenna Arrays

Plasmonic nano-antennas and nano-antenna arrays are not just the miniaturization of traditional metallic antennas or antenna arrays. Plasmonic materials are metals or metal-like materials which support the propagation of Surface Plasmon Polariton (SPP) waves. SPP waves are confined electromagnetic (EM) waves that appear at the interface between a metal and a dielectric as a result of global oscillations of the electrical charges. Different plasmonic materials can support SPP waves at different frequencies. In this paper, we continue our studies on graphene [6], [8] to build UM MIMO systems.

The unique propagation properties of SPP waves enable the development of novel plasmonic nano-antennas. In particular, SPP waves propagate at a much lower speed than EM waves in free space. As a result, the SPP wavelength λ_{spp} is much smaller than the free-space wavelength λ. The ratio

$$\gamma = \lambda/\lambda_{\text{spp}} \tag{1}$$

is known as the confinement factor and depends on the plasmonic material and the system frequency. The confinement factor γ can be obtained by solving the SPP wave dispersion equation with the boundary conditions imposed by the specific device geometry [8]. In this paper, we consider graphene-based plasmonic nano-patch antennas, composed of a graphene layer on top a metallic ground plane, with a dielectric material in between. The dispersion equation for Transverse Magnetic (TM) SPP waves on gated graphene structures in the quasi-static regime is

$$\frac{\varepsilon_1 + \varepsilon_2 \coth\left(k_{spp} d\right)}{k_{spp}} + i\frac{\sigma_g}{\omega\varepsilon_0} = 0, \tag{2}$$

where $k_{spp} \gg \omega/c$ and c is the speed of light. σ_g is the well-known conductivity of graphene [9], ε_1 is the relative permittivity of the dielectric above the graphene layer, and ε_2 is the relative permittivity of the dielectric between the graphene layer and the metallic ground plane, which are separated by a distance d.

By solving (2), the complex wave vector k_{spp} can be obtained. While a closed-form expression for k_{spp} does not exist, it can be obtained numerically. The real part of the wave vector $\text{Re}\{k_{spp}\}$ determines the SPP wavelength λ_{spp}

$$\lambda_{\text{spp}} = \frac{2\pi}{\text{Re}\{k_{spp}\}}, \tag{3}$$

whereas the imaginary part, $\text{Im}\{k_{spp}\}$, determines the SPP decay or, inversely, the propagation length $\mathcal{L}$ is

$$\mathcal{L} = \frac{1}{2\,\text{Im}\{k_{spp}\}}, \tag{4}$$

which is defined as the distance at which the SPP intensity has decreased by a value of $1/e$.

Finally, different from metallic antennas, the resonance length of a plasmonic antenna is given by

$$l_p \approx \lambda_{\text{spp}}/2 = \lambda/\left(2\gamma\right), \tag{5}$$

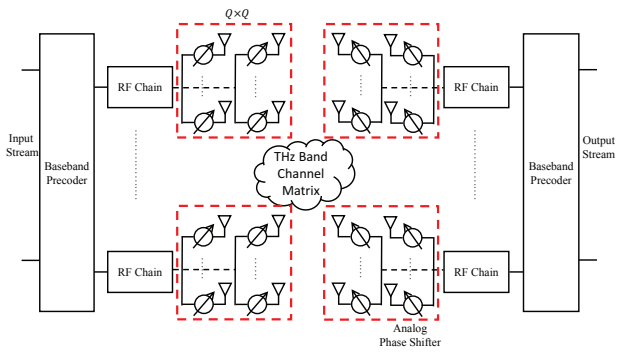

Fig. 1. UM-MIMO based on the array-of-subarray (AoSA) structure with hybrid beamforming. Each subarray is composed of $Q \times Q$ tightly packed antenna elements.

and, thus, plasmonic antennas are much smaller than the metallic antennas. For example, the confinement factor γ in graphene ranges between 10 to 100. As a result, graphene-based plasmonic nano-antennas are just a few micrometers long and only hundreds of nanometers wide, i.e., almost two orders of magnitude smaller than the metallic THz antennas. On the one hand, this result leads to much denser antenna arrays, with up to thousands of elements within millimetric footprints [5]. On the other hand, however, the control of the array becomes a challenging task. While the very small size of individual THz plasmonic nano-transceivers [6] would allow the development of a fully digital architecture, the control of each individual nano-transceiver would become a challenge.

B. Grouping and Control of Plasmonic Nano-antenna Arrays

The conceptual design of an end-to-end UM MIMO system based on the AoSA architecture with hybrid beamforming [10] is illustrated in Fig. 1. In particular, $M_t \times N_t$ and $M_r \times N_r$ antenna subarrays are equipped at the transmitter (Tx) and the receiver (Rx), respectively, in which each subarray is driven by an individual baseband-to-RF chain. Then, each subarray is composed of $Q \times Q$ tightly packed antenna elements. Each antenna element is connected to a time-delay control line (broadband phase shifter) which can be implemented by digitally controlled graphene integrated gates. In the AoSA structure, the basic component in the THz system becomes a subarray rather than an antenna element. The beamforming gain enabled in an individual subarray contributes to overcoming the very high path loss at THz frequencies.

III. UM-MIMO Channel Model

In this section, we develop a complete channel model for UM-MIMO communications based on the AoSA structure. More specifically, we utilize ray-tracing techniques to develop a channel model that takes into account the 3D propagation in the THz band, the nano-antenna array factor and the mutual coupling between neighboring nano-antennas.

Let $\boldsymbol{x}$ be the $N_s \times 1$ input symbol vector and $\boldsymbol{n}$ be the $M_r N_r \times 1$ noise signal vector at the receiving subarrays, the end-to-end UM-MIMO communication model is given as a

function of the frequency f,

$$\boldsymbol{y}(f) = \boldsymbol{w}_r^{\dagger}(f)\boldsymbol{H}_{\mathrm{UM}}(f)\boldsymbol{w}_t(f)\boldsymbol{x}(f) + \boldsymbol{w}_r^{\dagger}(f)\boldsymbol{n}(f), \quad (6)$$

where $\boldsymbol{y}$ is the $N_s \times 1$ received symbol vector, $\boldsymbol{w}_t \in R^{M_t N_t \times Ns}$ and $\boldsymbol{w}_r \in R^{M_r N_r \times Ns}$ are the baseband precoder and combiner vectors at the transmitter and receiver, which can dynamically adapt the utilization of the subarrays. $\boldsymbol{H}_{\mathrm{UM}}$ is the $M_r N_r \times M_t N_t$ transfer function matrix in UM-MIMO systems. The operator $(\cdot)^{\dagger}$ denotes the conjugate transpose.

As an element in the matrix $\boldsymbol{H}_{\mathrm{UM}}$, the frequency response between the (m_t, n_t) transmitting and the (m_r, n_r) receiving subarrays is described as

$$H_{m_r n_r, m_t n_t}(f) = \boldsymbol{a}_r^{\dagger}(\phi_r, \theta_r) G_r \alpha_{m_r n_r, m_t n_t}(f) G_t \boldsymbol{a}_t(\phi_t, \theta_t), \quad (7)$$

where between the (m_t, n_t) transmitting and the (m_r, n_r) receiving subarrays, $\alpha_{m_r n_r, m_t n_t}$ is the path gain, $\boldsymbol{a}_t$/$\boldsymbol{a}_r$ stand for the subarray steering vectors of the transmitting/receiving subarray, and G_r/G_t are the gains of transmitting/receiving antennas. Moreover, the angle-of-departure and angle-of-arrival are denoted by ϕ_t, θ_t and ϕ_r, θ_r, where ϕ_t and ϕ_r are the azimuth angles and θ_t and θ_r are the elevation angles.

A. Path Gain

Based on our prior work [7], the main components of the THz channel are of line-of-sight (LoS) and the non-line-of-sight (NLoS) reflected rays, while the other multi-path effects such as scattering and diffraction have significantly less contribution to the received signal power. Furthermore, benefiting from the the beamforming gain in the AoSA architecture, we consider that only one dominant ray travels between a transmitting subarray and a receiving subarray. Therefore, the path gain is computed through either the LoS or a reflected path, similarly as in mm-wave systems [11].

At THz frequencies, the path gain of the LoS propagation α_{LoS} depends on the spreading loss and the molecular absorption loss [3],

$$\alpha_{\mathrm{LoS}}(f) = \frac{c}{4\pi f d} \exp\left(-\frac{1}{2}\mathcal{K}(f) d\right) \exp\left(-j2\pi f \tau_{\mathrm{LoS}}\right), \quad (8)$$

where c stands for the speed of light, and d represents the traveling distance. The time-of-arrival (ToA) of the LoS path is $\tau_{\mathrm{LoS}} = d/c$. The molecular absorption coefficient, $\mathcal{K}$, is frequency-selective and accounts for the attenuation resulting from the fact that part of the wave energy is converted into internal kinetic energy of the molecules in the propagation medium [3].

For the NLoS path, if we denote R as the the reflection coefficient, r_1 as the distance between the transmitter and the reflector, and r_2 as the distance between the reflector and the receiver, the path gain for the reflected ray α_{Ref} is given by

$$\alpha_{\mathrm{Ref}}(f) = \frac{c}{4\pi f\,(r_1 + r_2)} \cdot \exp\left(-\frac{1}{2}\mathcal{K}(f)\,(r_1 + r_2)\right) \cdot R(f) \exp\left(-j2\pi f \tau_{\mathrm{Ref}}\right), \quad (9)$$

where $\tau_{\mathrm{Ref}} = \tau_{\mathrm{LoS}} + (r_1 + r_2 - d)/c$ is the time-of-arrival of the reflected ray.

Based on (8) and (9), the path gain between the (m_t, n_t) transmit subarray and the (m_r, n_r) receive subarray in (7) depends on the path type and is equal to

$$|\alpha_{m_r n_r, m_t n_t}(f)| = \begin{cases} |\alpha_{\mathrm{LoS}}(f)| & \text{LoS,} \\ |\alpha_{\mathrm{Ref}}(f)| & \text{Reflected path.} \end{cases} \quad (10)$$

B. Subarray Steering Vector

The subarray steering vector is distorted by the mutual coupling effect, and is influenced by the phase shift of the antenna elements in the subarray. The subarray steering vectors for Tx and Rx are expressed as

$$\boldsymbol{a}_t(\phi_t, \theta_t) = \boldsymbol{C}_t \boldsymbol{a}_0(\phi_t, \theta_t), \quad (11)$$

$$\boldsymbol{a}_r(\phi_r, \theta_r) = \boldsymbol{C}_r \boldsymbol{a}_0(\phi_r, \theta_r), \quad (12)$$

where $\boldsymbol{C}_t, \boldsymbol{C}_r \in R^{N_{sa} \times N_{sa}}$ represent the mutual coupling matrices of the graphene-based nano-antenna arrays at Tx and Rx respectively, which were investigated in our prior work [12]. In this analysis, we will consider the separation between antennas to be larger than λ_{spp}, and, thus, the coupling is negligible. Let $N_{sa} = Q \times Q$ be the number of antennas in each subarray. Moreover, $\boldsymbol{a}_0$ stands for the ideal subarray steering vector in a uniform planar array.

In a subarray with $Q \times Q$ antenna elements, the ideal subarray vector $\boldsymbol{a}_0$ is described as a function of the azimuth angle ϕ and the elevation angle θ as

$$\boldsymbol{a}_0(\phi, \theta) = \frac{1}{Q}\left[e^{j\Phi_{1,1}}, \ldots, e^{j\Phi_{1,Q}}, e^{j\Phi_{2,1}}, \ldots, e^{j\Phi_{p,q}}, \ldots, e^{j\Phi_{Q,Q}}\right]^T, \quad (13)$$

where the operator $(\cdot)^T$ denotes the transpose. The phase shifts of the antenna element (p, q) in the subarray is

$$\Phi_{p,q}(\phi, \theta) = d_x^{(p,q)}\Psi_x(\phi, \theta) + d_y^{(p,q)}\Psi_y(\phi, \theta) + d_z^{(p,q)}\Psi_z(\phi, \theta). \quad (14)$$

$$\Psi_x(\phi, \theta) = \frac{2\pi}{\lambda_{\mathrm{spp}}} \cos\phi \sin\theta, \quad (15)$$

$$\Psi_y(\phi, \theta) = \frac{2\pi}{\lambda_{\mathrm{spp}}} \sin\phi \sin\theta, \quad (16)$$

$$\Psi_z(\phi, \theta) = \frac{2\pi}{\lambda_{\mathrm{spp}}} \cos\theta. \quad (17)$$

In (14), $d_x^{(p,q)}$, $d_y^{(p,q)}$ and $d_z^{(p,q)}$ are coordinate positions in the $x-$, $y-$ and $z-$axis in the 3D environment, for the antenna element (p, q) of the subarray.

By grouping the antenna elements in a subarray for beamforming as discussed in Sec. II-B, the phase shifts in (13) of the subarray in Tx and Rx that direct to the desired angle directions (ϕ_t, θ_t) and (ϕ_r, θ_r) in (7) are

$$\Omega_t^{(p,q)} = d_x^{(p,q)}\Psi_x(\phi_t, \theta_t) + d_y^{(p,q)}\Psi_y(\phi_t, \theta_t) + d_z^{(p,q)}\Psi_z(\phi_t, \theta_t), \quad (18)$$

$$\Omega_r^{(p,q)} = d_x^{(p,q)}\Psi_x(\phi_r, \theta_r) + d_y^{(p,q)}\Psi_y(\phi_r, \theta_r) + d_z^{(p,q)}\Psi_z(\phi_r, \theta_r), \quad (19)$$

where $\Omega_t^{(p,q)}$ and $\Omega_r^{(p,q)}$ stand for the phase shifts of the (p,q) antenna elements in the subarray at Tx and Rx, respectively.

IV. UM-MIMO Channel Characterization

The developed UM-MIMO channel is characterized and evaluated in this section, by focusing on the path gain, the array factor and the the wideband capacity for both spatial multiplexing and beamforming regimes.

A. Properties of Plasmonic Nano-antennas

The size of graphene-based plasmonic nano-antennas are determined by the confinement factor (1), which depends on the SPP wave vector k_{spp} and can be numerically obtained by solving the dispersion equation given by (2). On its turn, k_{spp} depends on the conductivity of the graphene layer σ_g, which changes with the Fermi energy, E_F, of the structure. In Fig. 2, the confinement factor (1) is shown as a function of frequency for different values of the Fermi energy. More specifically, we consider a structure consisting of a graphene layer with E_F ranging from 0.1 electronVolts (eV) to 0.5 eV and relaxation time $\tau_g = 0.1$ ps at room temperature (300 K), on top of a metallic ground plane with a 90 nm-thick SiO_2 dielectric in between ($\varepsilon_1 = 1, \varepsilon_2 = 4$).

The remarks regarding the properties of graphene-based nano-antennas are summarized as follows. First, the confinement factor (1) decreases with the operating frequency. At 1 THz and $E_F = 0.5$eV, the confinement factor is 15, which suggests that the SPP wavelength λ_{spp} is $1/15$ of the free-space wavelength. As a result, many additional graphene-based nano-antennas can be embedded in the same footprint to enable UM-MIMO systems in the THz band. Moreover, as the Fermi energy increases from $0.1, 0.2$ to 0.5 eV, the confinement factor decreases from 32, 24 to 15. At a given operating frequency, the resonance length of a plasmonic antenna given by (5) increases with the Fermi energy.

B. Dimensions of the UM-MIMO System

The dimensions of the UM-MIMO system are set by the size of the plasmonic nano-antenna arrays. The latter depends on both the size of each nano-antenna as well as the minimum separation between two consecutive elements. For the former, as discussed in Sec. II-A, we consider the antenna length and width to be equal to $\lambda_{\text{spp}}/2$. For the latter, as discussed in Sec. II-B, in order to limit the impact of mutual coupling between neighboring elements, we consider the separation between two elements to be one plasmonic wavelength λ_{spp}. Then, by considering the subarray size equal to $Q \times Q = 8 \times 8$, with f=1 THz and E_F=0.5 eV ($\gamma = 15$), the number of sub-arrays per dimension is $N_{sa,1d} = 4$ and, therefore, the total number of antennas in the array is $(4 \times 8) \times (4 \times 8) = 1024$. On the contrary, to pack the same number of metallic antennas, a footprint size of 2.07 cm^2 is required, which is more than 200 times larger than the area required for the plasmonic nano-antenna array. This is due to the fact that the equivalent electrical size of a graphene antenna is much larger than its physical dimensions, owing it to the much lower speed of SPP waves in a graphene-based antenna compared to that of free-space EM waves in a metallic antenna.

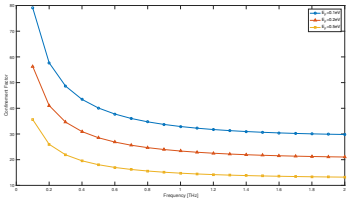

Fig. 2. Confinement factor γ for different Fermi energy (d=90 nm, ε_1=1, ε_2=4).

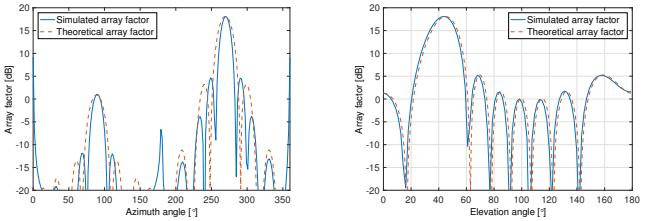

(a) Azimuth plane (b) Elevation plane

Fig. 3. Array factor in the UM-MIMO, with the subarray size of 8×8. The operating frequency is 1 THz.

C. Array Factor

The array factor given by (13) is shown in Fig. 3 for both the azimuth and the elevation planes. To validate the theoretical study, we conduct extensive numerical simulations with COMSOL Multi-physics, a fine-element-method simulation engine. The main beam is directed to $270°$ and $45°$, in the azimuth (see Fig. 3(a)) and elevation (see Fig. 3(b)) planes, respectively. At 1 THz, the subarray size of 8×8 can provide 18 dB gain. The antenna spacing is half wavelength and the mutual coupling effects are not included. The sidelobes decay quickly, maintaining below 5 dB. The theoretical results match well with the COMSOL curves, which proves that the analysis in Sec. III-B accurately captures the properties of the subarray steering vector.

D. Wideband Channel Capacity

Enabled by the large size of antenna arrays and thanks to the array-of-subarray architecture described in Sec. II-B, the UM-MIMO system could be used for either beamforming or spatial multiplexing [5].

On the one hand, the UM-MIMO system with the multiple subarrays can support multi-stream communication adopting the *spatial multiplexing* mechanisms. The UM-MIMO channel capacity with spatial multiplexing is numerically evaluated in Fig. 4, for the different number of subarrays and transmit power. The subarray size is 8×8, and the distance is 20 m. In the regime of spatial multiplexing, the number of data streams is equal to the number of subarrays in the UM-MIMO, aiming to maximize the achievable rates over the THz channel. In the $0.3 - 0.4$ THz spectral window, 10 Tbps is achievable when the number of subarrays exceeds 8. Although the capacity increases as the transmit power increases from 1 dBm to

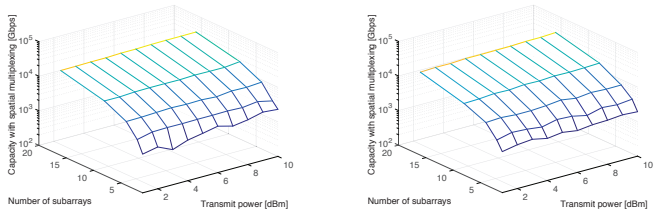

(a) Spectral window $0.3-0.4$ THz (b) Spectral window $0.9-1$ THz

Fig. 4. UM-MIMO capacity with spatial multiplexing, for the different number of subarrays and transmit power (subarray size 8×8, distance 20 m).

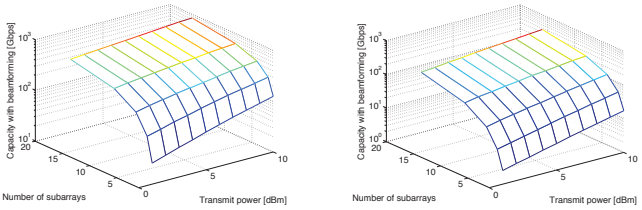

(a) Spectral window $0.3-0.4$ THz (b) Spectral window $0.9-1$ THz.

Fig. 5. UM-MIMO capacity with beamforming, for the different number of subarrays and transmit power (subarray size 8×8, distance 20 m).

10 dBm, the impact is slighter than the increases of the number of the subarray. This can be explained that additional data streams are enabled with the increase of the number of the subarray, which improves the capacity substantially. On the other hand, the capacity in the $0.9-1$ THz spectral window is reduced. In particular, the largest capacity with 16 subarrays and the transmit power at 10 dBm drops from 33 Tbps to 30 Tbps, by increasing the frequency from 0.3 THz to 1 THz.

On the other hand, the large number of subarrays are grouped together and is capable of steering high-gain narrow beams towards the strongest propagation path, as beamforming. This beamforming design can effectively overcome the very high attenuation at the THz frequencies and importantly, enhance the communication distance. Particularly in the THz systems, the transmission power is limited while the bandwidth resource is sufficient, beamforming may provide greater capacity by increasing the SNR.

The UM-MIMO channel capacity is shown in Fig. 5, for the different number of subarrays and transmit power. In Fig. 5(a), the spectral window of $0.3-0.4$ THz is utilized, which yields a larger capacity compared to Fig. 5(b) in which $0.9-1$ THz is adopted. Although the bandwidth is the same, the path loss increases as the frequency increases, which results in the decrease of the SNR, and consequently the capacity. The largest capacity reaches 0.8 Tbps, when 16 subarrays are included in the UM-MIMO system and the transmit power is 10 dBm. Compared to the results with the spatial multiplexing (see Fig. 4), the capacity with beamforming is degraded by one order of magnitude. This is reasonable since the focus of the beamforming technique is to improve the SNR and overcome the distance limitation, rather than maximizing the achievable rates. Interestingly, although the path loss increases as the frequency increases, the antenna array size decreases thanks to the smaller wavelength. Therefore, more subarrays could be accommodated in a given footprint size, which can compensate for the higher path loss.

V. Conclusion

In this paper, we have developed a channel model for UM-MIMO systems using the AoSA architecture. The properties of the graphene-based plasmonic nano-antenna arrays and the 3D THz propagation phenomena have been taken into account. We have presented an extensive characterization on the graphene antenna and UM-MIMO propagation channel.

Acknowledgement:

This work was supported by the U.S. NSF under Grant No. ECCS-1608579 and in part by Alexander von Humboldt Foundation through Prof. Akyildiz's Humboldt Research Prize in Germany.

This work was also supported by the U.S. National Science Foundation under Grant CNS-1730148.

This work was also supported by National Natural Science Foundation of China (NSFC) under Grant No. 61701300 and Shanghai Sailing (YANG FAN) Program under Grant No. 17YF1409900.

References

[1] J. Federici and L. Moeller, "Review of terahertz and subterahertz wireless communications," *Journal of Applied Physics*, vol. 107, no. 11, p. 111101, 2010.

[2] I. F. Akyildiz, J. M. Jornet, and C. Han, "Terahertz band: Next frontier for wireless communications," *Physical Communication (Elsevier) Journal*, vol. 12, pp. 16–32, Sep. 2014.

[3] J. M. Jornet and I. F. Akyildiz, "Channel modeling and capacity analysis of electromagnetic wireless nanonetworks in the terahertz band," *IEEE Transactions on Wireless Communications*, vol. 10, no. 10, pp. 3211–3221, Oct. 2011.

[4] E. Larsson, O. Edfors, F. Tufvesson, and T. Marzetta, "Massive MIMO for next generation wireless systems," *IEEE Communications Magazine*, vol. 52, no. 2, pp. 186–195, 2014.

[5] I. F. Akyildiz and J. M. Jornet, "Realizing Ultra - Massive MIMO (1024x1024) Communication in the (0.06 - 10) Terahertz Band," *Nano Communication Networks (Elsevier) Journal*, vol. 8, pp. 46–54, 2016.

[6] J. M. Jornet and I. F. Akyildiz, "Graphene-based plasmonic nano-transceiver for terahertz band communication," in *Proc. of European Conference on Antennas and Propagation (EuCAP)*, 2014.

[7] C. Han and I. F. Akyildiz, "Three-Dimensional End-to-End Modeling and Analysis for Graphene-Enabled Terahertz Band Communications," *IEEE Transactions on Vehicular Technology, special section on THz Communication for Vehicular Networks*, 2017.

[8] J. M. Jornet and I. F. Akyildiz, "Graphene-based plasmonic nano-antenna for terahertz band communication in nanonetworks," *IEEE JSAC, Special Issue on Emerging Technologies for Communications*, vol. 12, no. 12, pp. 685–694, Dec. 2013.

[9] L. Falkovsky and A. A. Varlamov, "Space-time dispersion of graphene conductivity," *The European Physical Journal B*, vol. 56, pp. 281–284, 2007.

[10] C. Lin and G. Y. L. Li, "Terahertz communications: An array-of-subarrays solution," *IEEE Communications Magazine*, vol. 54, no. 12, pp. 124–131, 2016.

[11] E. Torkildson, U. Madhow, and M. Rodwell, "Indoor millimeter wave MIMO: Feasibility and performance," *IEEE Transactions on Wireless Communications*, vol. 10, no. 12, pp. 4150–4160, 2011.

[12] L. Zakrajsek, E. Einarsson, N. Thawdar, M. Medley, and J. M. Jornet, "Design of Graphene-based Plasmonic Nano-antenna Arrays in the Presence of Mutual Coupling," in *Proc. of the 11th European Conference on Antennas and Propagation (EuCAP)*, 2017.